Bioorganic Chemistry 93 (2019) 103307

Contents lists available at ScienceDirect

Bioorganic Chemistry

journal homepage: www.elsevier.com/locate/bioorg

Design, synthesis, molecular modelling, ADME prediction and anti-hyperglycemic evaluation of new pyrazole-triazolopyrimidine hybrids as potent α-glucosidase inhibitors

Vinay Pogaku[a], Kiran Gangarapu[b], Srinivas Basavoju[a,*], Kiran Kumar Tatapudi[c], Suresh Babu Katragadda[c]

[a] Department of Chemistry, National Institute of Technology, Warangal 506004, Telangana, India
[b] Department of Pharmaceutical Chemistry, School of Pharmacy, Anurag Group of Institutions, Hyderabad 500088, Telangana, India
[c] Centre for Natural Products & Traditional Knowledge, CSIR-Indian Institute of Chemical Technology, Hyderabad 500007, India

ARTICLE INFO

Keywords:
α-Glucosidase inhibition activity
Triazolopyrimidines
Multicomponent approach
Molecular docking
ADME studies

ABSTRACT

The aim of the present study is to design and synthesis of new pyrazole-triazolopyrimidine hybrids as potent α-glucosidase inhibitors. The target compounds **4a-n** were synthesized by one-pot multicomponent approach with good yields and were characterized by various spectroscopic techniques and finally by single crystal X-ray diffraction method (**4j**). All the newly-synthesized derivatives have been screened for their α-glucosidase enzyme inhibition activity and acarbose taken as a standard drug. Among all the tested compounds, **4h** has displayed excellent α-glucosidase enzyme inhibition activity with IC_{50} value 12.45 μM to the standard drug acarbose (IC_{50}: 12.68 μM). Similarly, the compounds **4f** and **4l** have exhibited potent activity with IC_{50} values 14.47 μM and 17.27 μM respectively. Structure-activity relationship (SAR) studies of all the title compounds were established. The mode of binding interactions between the α-glucosidase enzyme and the compounds were studied. The drug-likeness properties (Lipinski parameters and *in silico* ADME properties) have predicted for the target compounds. The α-glucosidase inhibition, molecular docking and drug-likeness properties of the compounds **4h**, **4f** and **4l** were suggested that these are promising hits for anti-diabetic activity.

1. Introduction

Diabetes mellitus is related to metabolic disorder, currently it became a major health problem around the world [1,2]. International Diabetes Federation (IDF), estimated that 415 million people were affected by this disease in 2015 and this number may increase to 642 million by 2040 [3–5]. The major form of diabetes is type-2 which is characterized by insulin resistance leads to the abnormal glucose levels in the blood called hyperglycemia [6]. Hyperglycemia condition causes damage to various physiological processes in the body. D-glucose releases from the nonreducing end of the substrate by the hydrolase of the glucosidic O-linkage with the help of α-glucosidase enzyme [7]. α-Glucosidase inhibitors prevent the hydrolysis of oligo or polysaccharides to glucose and thus reduce the postprandial rise of blood glucose [8]. Inhibition of α-glucosidase enzyme in the digestive system is one of the best options to maintain postprandial glucose level by delaying carbohydrate absorption [9]. The clinically used anti-diabetic drugs are effectively decreasing the glucose levels in type-2 diabetic patients. However, these drugs associated to side effects like flatulence, diarrhea and abdominal discomfort [10,11]. Hence, there is an urgency to the design and development of new α-glucosidase inhibitors with higher efficacy and non-toxic nature.

In this context, pyrazole scaffolds have been reported as potent anti-diabetic agents in the literature [12]. Pyrazole containing natural amino acid L-α-amino-β-(pyrazolyl-N)-propanoic acid isolated from *Citrullus vulgaris* has potential anti-diabetic activity [13]. Later, several entities of the pyrazole have been reported to possess potent anti-diabetic activity. For instance, pyrazole containing compound **A** (shown in Fig. 1) exhibited potent α-glucosidase inhibition activity [14]. Kenneth et al. reported the pyrazole and pyrazolone derivatives as potent anti-hyperglycemic agents for the treatment of diabetes [15] and Shuangjie et al. described the pyrazole containing derivatives as a potent glucagon receptor antagonist [16,17]. The pyrazole heterocycles are also known to possess many other biological activities like anti-inflammatory, antimicrobial, anticancer and cyclooxygenase-2 inhibitor activities [18].

Similarly, triazole and triazolopyrimidine derivatives are important

* Corresponding author.
E-mail address: basavojusrinivas@nitw.ac.in (S. Basavoju).

https://doi.org/10.1016/j.bioorg.2019.103307
Received 25 June 2019; Received in revised form 13 September 2019; Accepted 19 September 2019
Available online 20 September 2019
0045-2068/

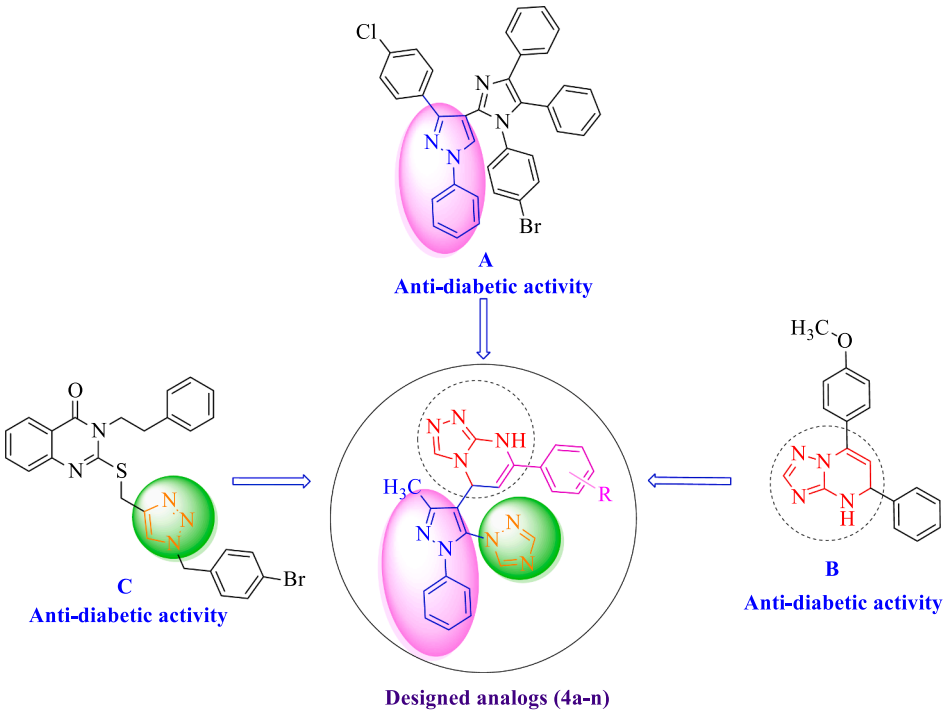

Fig. 1. The design strategy of new pyrazole-triazolopyrimidine hybrids as new α-glucosidase inhibitors based on molecular hybridization of pharmacophoric units of potent reported α-glucosidase inhibitors **A–C**.

analogues and exhibit the applications in drug discovery and medicinal chemistry [19,20]. The triazole linked compounds (Fig. 1. compound C) have shown good α-glucosidase activity [21]. Satya and Shazia et al. have reported triazole based derivatives as potent α-glucosidase inhibitors [22,23]. Triazolopyrimidines (Fig. 1. compound B) have been used for the treatment of diabetes as phosphodiesterase inhibitors through selective inhibition of dipeptidyl peptidase-4 (DPP4) [24–26]. DeNinno et al. discovered the triazolopyrimidine based PDE8B inhibitors for the treatment of diabetes [26]. Apart from this, triazolopyrimidines display many biological activities [27–30]. In light of above, and also as a part of our interest towards the search of novel potent biologically active heterocyclic hybrids [31,32], we opted to design a new hybrid moiety that embodied pyrazole, triazole and triazolopyrimidine in a single frame *via* multicomponent approach and explored their anti-diabetic activity.

2. Results and discussion

2.1. Chemistry

The starting material 3-methyl-1-phenyl-5-(1*H*-1,2,4-triazol-1-yl)-1*H*-pyrazole-4-carbaldehyde **1** was prepared by the nucleophilic substitution of 5-chloro-3-methyl-1-phenyl-1*H*-pyrazole-4-carbaldehyde with 1*H*-1,2,4-triazole under reflux condition in DMF and anhydrous K_2CO_3 for 4 h [33]. In order to optimize the reaction condition for the synthesis of the title compounds **4a-n**, a pilot reaction was carried out by taking the trial reactants 3-methyl-1-phenyl-5-(1*H*-1,2,4-triazol-1-yl)-1*H*-pyrazole-4-carbaldehyde **1**, acetophenone **2a** and 4*H*-1,2,4-triazol-3-amine **3**. The optimization results of the compound **4a** were summarized in Table 1.

Initially, the reaction was carried out in different solvents such as methanol, ethanol, acetonitrile and dimethylformamide (DMF) under reflux condition resulting the product **4a** with poor yields (Table 1, entries 1–4). Then, the reaction was tried in piperidine under reflux condition and observed that the compound **4a** was formed with 78% yields in DMF solvent which is high compared to the other solvents (Entry 5–8). Later, the reaction was carried out in DMF with different bases such as triethylamine (TEA), DABCO and pyridine under reflux condition resulted in the product **4a** with yields of 42%, 49% and 54% respectively (Entry 9–11). However, piperidine is high in terms of the yield and reaction time compared to the other bases.

Further, in order to optimize the reaction condition, piperidine with different equivalents were tried. Notably, the reaction with 1.5 equivalents of piperidine gave the desired product **4a** with a higher yield of 88% in 8 h and it was considered as the best-optimized reaction condition for the synthesis of target compounds derivatives **4a-n**. Later, this reaction condition was successfully executed to synthesize the compounds **4a-n** using various substituted acetophenones. Further, the final products were purified by the column chromatography. The compounds **4a-n** were obtained in 6–10 h and yields ranging from 70 to 88% were depicted in table 2.

The possible mechanism for the synthesis of the new pyrazole-triazolopyrimidine hybrid derivatives **4a-n** was shown in Scheme 1. Initially, 3-methyl-1-phenyl-5-(1*H*-1,2,4-triazol-1-yl)-1*H*-pyrazole-4-carbaldehyde **1** under goes Knoevenagel condensation with aromatic acetophenone to form the chalcone **5**. Then, the 4*H*-1,2,4-triazol-3-amine **3** attacks on chalcone intermediate **5** to form intermediate **6**, In the next step, **6** is converted to **7** *via* an intramolecular cyclization, followed by the dehydration to provides the target compounds.

The structures of all the synthesized compounds were well characterized by ^{1}H NMR and ^{13}C NMR, IR, mass spectral data and single crystal X-ray diffraction method (**4j**). For instance, the IR spectrum of **4j** showed a band at 3435 cm^{-1} corresponds to the N—H group of the pyrimidine ring. In the ^{1}H NMR, the peak showed at δ 10.14 corresponds to N—H proton of the pyrimidine ring. The characteristic peaks appeared at δ 6.09 and 5.02 corresponds to the two protons attached to the C10, C11 carbons (Fig. 3). The ^{13}C NMR spectrum showed the peaks at δ 94.52 and 51.25 corresponds C10, C11 carbons of pyrimidine ring (Fig. 3). Further, MS/MS spectra of the compounds (**4h**, **4j**, **4 k** and **4 m**) were reported and consequently, the fragmentation pathway were reported (see supporting information). Here present MS/MS spectrum and fragmentation pattern of the compound **4j** (Fig. 2 and Scheme 2).

The above all the spectral data confirms the structures of the compounds **4a-n** and further confirmed by the single crystal X-ray

Table 1
Optimization conditions of the reaction parameters for the synthesis of **4a**.

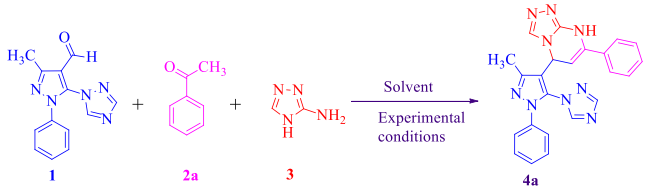

[a]Entry	Solvent	Base	Time (h)	[b]Yield (%)
1	Methanol	–	24	15
2	Ethanol	–	24	20
3	ACN	–	24	24
4	DMF	–	24	40
5	DMF	Piperidine, 1 eq	8	78
6	Methanol	Piperidine, 1 eq	20	42
7	Ethanol	Piperidine, 1 eq	20	49
8	ACN	Piperidine, 1 eq	18	54
9	DMF	TEA, 1 eq	9	65
10	DMF	Pyridine, 1 eq	14	58
11	DMF	DABCO, 1 eq	10	62
12	DMF	Piperidine, 1.5 eq	8	88
13	DMF	Piperidine, 2.0 eq	8	84

[a] Reaction conditions: compound **1** (1 mmol), acetophenone **2a** (1 mmol), 4*H*-1,2,4-triazol-3-amine **3** (1 mmol) and solvent under reflux condition.
[b] Isolated yields. Eq = equivalent.

diffraction method (**4j**). The salient features of crystallographic information and the CCDC number (1936467) of the compound **4j** have shown in Table 3. The ORTEP representation of the **4j** with the atom numbering scheme has shown in Fig. 3.

2.2. Anti-diabetic activity

2.2.1. α-Glucosidase inhibitory activity

The new class of synthesized non-glycosidic pyrazole-triazolopyrimidine hybrids **4a-n** was screened for their potency of α-glucosidase inhibitory activity against α-glucosidase enzyme [34,35] and acarbose was taken as a standard drug. The results were presented in Table 3 as IC_{50} values and the IC_{50} values were expressed in terms of μM. The IC_{50} values of the tested compounds ranged from 12.45 ± 0.59 to 52.58 ± 0.65 μM (Table 4) were calculated by statistical regression analysis. Among all the compounds, the compound **4h** exhibited the excellent α-glucosidase inhibition activity with the IC_{50} value 12.45 μM, which is equal to the α-glucosidase inhibition activity of the standard drug acarbose (IC_{50}: 12.68 μM). Similarly, the compounds **4f** and **4l** exhibited potent α-glucosidase inhibitory activity with IC_{50} values 14.47 and 17.27 μM. Further, the compounds **4 g**, **4n** and **4j** showed the significant activity with IC_{50} values 20.30 μM, 23.70 μM and 25.67 μM respectively. The compounds **4a**, **4d**, **4i** and **4 m** exhibited moderate potency (IC_{50} values ≤40 μM), while rest of the compounds exhibited weak inhibitory potency (IC_{50} values > 40 μM) against the enzyme α-glucosidase.

2.2.1.1. Structure-activity relationship (SAR) studies. The synthesized compounds possess triazole, pyrazole, pyrimidine ring and different substitutions on the phenyl ring have exhibited variable α-glucosidase inhibitory activity. Compounds substituted with electron withdrawing groups on the phenyl ring (**4h**, **4f**, **4l**, **4 g**, and **4n**) have displayed most potent inhibitory activity against the α-glucosidase enzyme. Among them compound **4h** with 4-Cl group has shown highest inhibition with IC_{50} value 12.45 μM and the compound **4f** with 4-floro group has shown with IC_{50} value 14.47 μM and followed by compound **4l** with 4-NO_2 μM has shown IC_{50} value 17.27 μM. Compounds substituted with electron donating groups (**4c**, **4d**, **4i** and **4 m**) have displayed moderate inhibitory activity. Compounds with unsubstituted on the phenyl ring have shown weak inhibitory activity. In this regard, it could be postulated that the compounds substitution on the phenyl ring would modulate the α-glucosidase inhibitory activity. Changing the position of the group on the phenyl ring has slightly modified the α-glucosidase inhibitory activity.

2.2.2. Molecular docking studies

In silico docking studies were carried out to explore the binding mode of ligands and were docked into the active site of α-glucosidase enzyme (PDB ID: 3WY1) by employing the GOLD 5.6 tool [36]. The crystal structure of the α-glucosidase enzyme (3WY1) contains two chains A and B and for the docking studies chain A has selected with co-crystal ligand Polyacrylic acid. The binding profile for pyrazole-triazolopyrimidine hybrids **4a-n** with α-glucosidase enzyme 3WY1 was determined and for each ligand ten conformations were generated. The conformation which is having the highest ranking was used for further analysis and gold fitness calculated using gold docking function. The gold score and interactions of the title compounds with receptors of the α-glucosidase protein 3WY1 have shown in Table 5.

All the compounds from this series **4a-n** have exhibited prominent gold fitness docking scores ranging from 45.78 to 89.75. The analysis of the compound **4h** (R = Chloro group) showed the highest gold score 89.45 and forms hydrogen bond, hydrophobic and van der waals interactions between compound **4h** and α-glucosidase protein. Hydrogen bonds are formed with residues and with distances Asp62 (2.57 Å), Asp333 (2.58 Å) and Asp202 (2.56 Å). It also forms short contacts with residues His105 (2.55), Phe166 (2.63) and Phe203 (2.76). These interactions are similar to the crystal ligand octane-1,3,5,7-tetracarboxylic acid with the following residues Arg400, Asp62, Arg200 Asp333 and Phe166. The nitrogen atom of the triazole ring was making a hydrogen bond with the oxygen atom of Asp 202 (2.56 Å). Moreover, the nitrogen atom of pyrazole ring was making a hydrogen bond with the oxygen atom of Asp62 (2.57 Å) and similarly Asp 333 forms two hydrogen bonds with the nitrogen atom of triazole and pyrimidine rings (Figs. 4 and 5).

The analysis of compound **4d** (R = OC_2H_5 group) showed next highest gold score 63.67 and forms hydrogen bond, hydrophobic and van der waals interactions between compound **4d** and α-glucosidase enzyme. Hydrogen bonds are formed with residues and with distances Arg200 (2.37), Glu271 (3.05), Gly228 (2.41) and Asp333 (2.62). It also forms short contacts with residues His105 (2.64), Phe166 (2.59), Arg333 (2.32) and Glu271 (2.39) (Fig. 4). The nitrogen atom of the

Table 2
Synthesis of pyrazole-triazolopyrimidine derivatives **4a-n**[a].

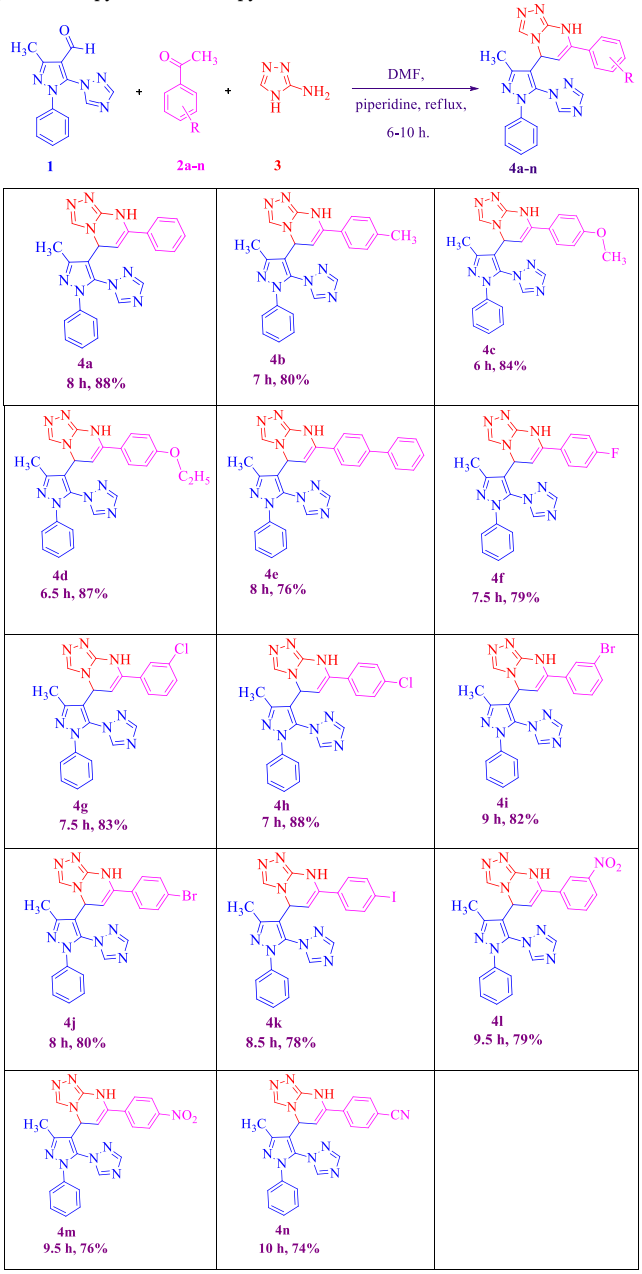

[a] Reaction conditions: compound **1** (1 mmol), acetophenone **2a-n** (1 mmol), 4*H*-1,2,4-triazol-3-amine **3** (1 mmol) in DMF (3 mL), piperidine (1.5 eq) under reflux condition.

triazole ring was making a hydrogen bond with oxygen atom of Arg200 (2.37 Å) and also with Asp333 (2.62). Moreover, the nitrogen atom of pyrimidine ring was making hydrogen bond with oxygen atom of Gly228 (2.41 Å) and similarly Glu271 forms hydrogen bonds with nitrogen atom of fused triazole ring (Fig. 4).

2.2.3. Computational analysis of Drug-likeness

The bioavailability of pyrazole-triazolopyrimidine derivatives (**4a-n**) was assessed through ADME (Adsorption, Distribution, Metabolism, and Excretion) using preADMET and molinspiration [37]. In order to explore drug-like properties of compounds (**4a-n**), the lipophilicity, expressed as the octanol/water partition coefficient and here it is called logP, as well as other theoretical calculations such as molecular size, the number of hydrogen bond acceptors and donors, TPSA and percentage of absorption as shown in Table 6.

The violation of more than one of the Lipinski parameters (Table 6) may indicate problems in the bioavailability of the potential drugs. The results showed that most of the compounds complied with Lipinski's rule (Table 6), with exception slightly high molecular size more than 500 of compounds **4i**, **4j** and **4k** and also some of the compounds like **4l** and **4 m** were found to be 12 hydrogen bond acceptors upon their predicted value (> 10). All the analogues have shown logP values less than 5 which demonstrating good membrane permeability. TPSA which ranges from 91.29 to 137.11 Å and found to be less than 140 Å which is a very useful parameter for the transport of drug molecule. Finally summarizing the physicochemical properties of these analogs (**4a-n**), we could conclude that almost they obey the rule-of-five of Lipinski rule and meet all criteria for good orally active diabetic drug.

2.2.4. ADME predictions

The major parameters for pharmacokinetics are absorption, distribution, metabolism and excretion [38]. The *in silico* ADME properties of all the compounds **4a-n** have shown satisfactory results. All the compounds have shown good intestinal absorption which are nearer to 100. The compounds have shown moderate permeability for *in vitro* Caco-2 cells ranges from 45.23 to 17.84 and low to moderate permeability for *in vitro* MDCK cells. Predicted *In vivo* blood-brain barrier penetration demonstrated that all the compounds have low absorption into the CNS and this indicates these compounds have less capability to cross the CNS. All the compounds have strong plasma protein binding value of more than 90% indicates strongly bound and also showed maximum skin permeability. Thus, from these results we observed that the synthesized pyrazole-triazolopyrimidine derivatives are having good drug likeliness and ADME property. The *in silico* predicted ADME properties and their values are shown in table 7.

3. Conclusion

New pyrazole-triazolopyrimidine hybrids **4a-n** were designed and synthesized with good yields by the multicomponent reaction. All the synthesized compounds were well characterized by IR, ^{1}H NMR, ^{13}C NMR, mass spectrometry and single crystal X-ray diffraction method (**4j**). The *in vitro* α-glucosidase inhibition activity of all the synthesized compounds was evaluated and six compounds were exhibited good α-glucosidase inhibition activity. Among these compounds, the compounds **4f** and **4l** have exhibited the potent activity with IC_{50} values 14.47 μM and 17.27 μM and particularly, the compound **4h** (IC_{50} = 12.45 μM) exhibited excellent α-glucosidase inhibition activity to the standard drug acarbose (IC_{50} = 12.68 μM). The compounds **4 g**, **4n** and **4j** have exhibited the significant activity with IC_{50} values 20.30 μM, 23.70 μM and 25.67 μM. SAR studies indicate that, the chloro, fluoro and nitro substitution on phenyl ring would favour for the α-glucosidase inhibitory activity. Further, the *in silico* studies of the title compounds with α-glucosidase protein (PDB ID: 3WY1) were studied, the compounds **4h**, **4l** and **4f** have shown the highest gold score (89.75, 63.18 and 57.30) which are highly correlated with *in vitro* α-glucosidase inhibition activity. The potent compounds **4h**, **4l** and **4f** were exhibited good Drug-likeness properties (ADME, Lipinski Parameters). Hence, these compounds could be promising hits for further development of new anti-diabetic drugs.

4. Experimental section

4.1. Chemistry

4.1.1. General procedure for the synthesis of title compounds 4a-n

A mixture of 3-methyl-1-phenyl-5-(1*H*-1,2,4-triazol-1-yl)-1*H*-pyrazole-4-carbaldehyde **1** (1 mmol), substituted acetophenones **2a-n** (1 mmol) and 4*H*-1,2,4-triazol-3-amine **3** (1 mmol) were taken in 5 mL of dimethylformamide and added 1.5 equivalent of piperidine then

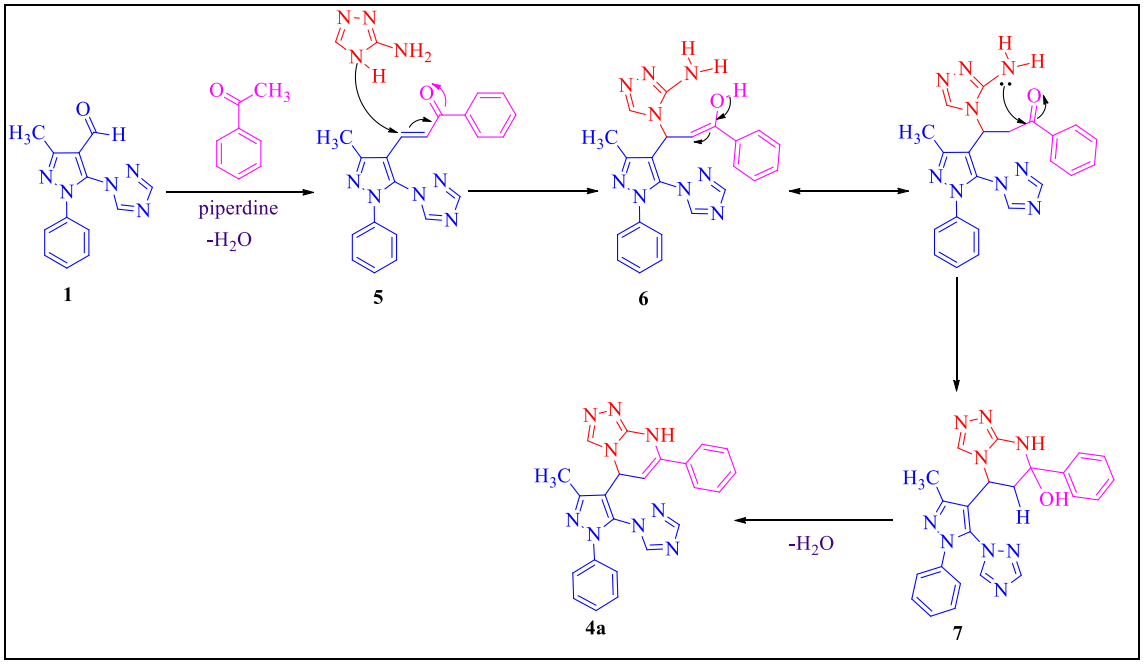

Scheme 1. The possible mechanism for the synthesis of the title compounds **4a-n**.

reflux the mixture for appropriate times (Tables 1 and 2). The progress of the reaction was monitored by TLC (eluent = *n*-hexane/ethyl acetate: 6/4). After completion of the reaction, the mixture was cooled to room temperature and added 20 mL of ice-cold water. The resulting solid was collected by filtration, washed with methanol and dried under vacuum. Further, the derivatives were purified by the column chromatography (*n*-hexane/ethyl acetate: 6/4).

4.1.2. General information

All the chemicals and solvents were purchased from Aldrich/Spectrochem. All melting points were checked by using Stuart SMP30 melting point apparatus (Bibby Scientific Ltd. United Kingdom) and were uncorrected. The reaction progress was checked with TLC plates (E. Merck, Mumbai, India) using UV light at 245 nm. Infrared spectra (IR) were recorded on KBr disc by using Perkin-Elmer 100S spectrophotometer (Perkin-Elmer Ltd. United Kingdom) from 400 to 4000 cm^{-1}. ^{1}H and ^{13}C NMR spectra were recorded on Avance-III Bruker-400 MHz spectrometer (400 MHz, Bruker Corporation Ltd., Germany) using $CDCl_3$, DMSO-d_6 as solvent and TMS as an internal standard, chemical shifts are expressed as ppm and coupling constants (*J* values) were given in hertz (Hz). The CHN analysis was recorded on Carlo Erba EA 1108 automatic analyzer (Triad, NJ, USA) and the values are ± 0.4% of theoretical values. Mass spectra were determined on a Jeol JMSD-300 spectrometer (Jeol Ltd., Tokyo, Japan) and *m/z* values were represented on x-axis, the intensity values were reported on y-axis.

4.1.3. Crystallographic data of compound 4j

CCDC 1936467 contains the supplementary crystallographic data (.cif) of the compounds **4j**. These data can be obtained free of charge from The Cambridge Crystallographic Data Centre via www.ccdc.cam.ac.uk/structures.

4.1.4. ESI-QTof-MS/MS condition

ToF-ESI-MS Experiments were carried on a Waters Xevo G2-XS time of flight (ToF) mass spectrometer (Waters, Milford, USA) connected to Waters H-Class inlet system. Spectra were acquired in ESI positive mode from *m/z* 50 to 1000. The capillary voltage set at 3 kV, sampling cone at

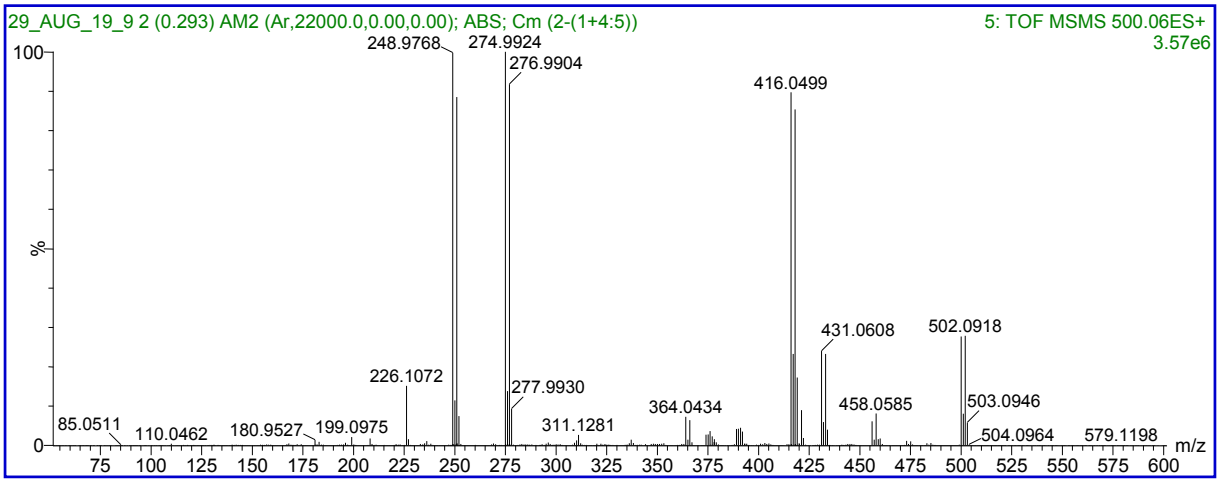

Fig. 2. TOF MS/MS spectra of the compound **4j**.

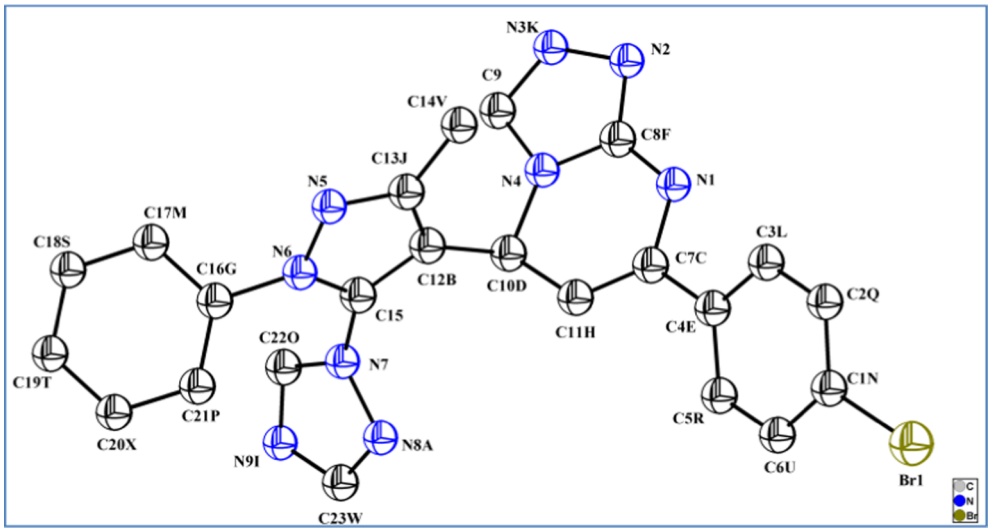

Fig. 3. ORTEP representation of compound **4j** and the thermal ellipsoids are drawn at 50% probability level.

40 and source temperature was set at 120 °C. ToF-MS/MS Experiments were performed at different collision energies varying from 10 V to 55 V where argon gas used for CID-MS/MS experiments. For ToF-MS and MS/MS analysis cone gas and desolvation gas (N_2) were set at 40 l/hr and 650 l/hr respectively with desolvation temperature adjusted at 300 °C. The inlet flow rate was adjusted at 0.1 mL/min with a mobile phase composition of water and acetonitrile mixed with 0.1% formic acid at a ratio of 15:85. Data processing and evaluation for MS experiments was performed with MassLynx v4.1 software SCN949 platform.

4.2. Biology

4.2.1. In vitro α-Glucosidase inhibitory activity

α-Glucosidase inhibitory activity was assayed by using 0.1 M phosphate buffer (pH 6.8) at room temperature [34,35]. The enzyme

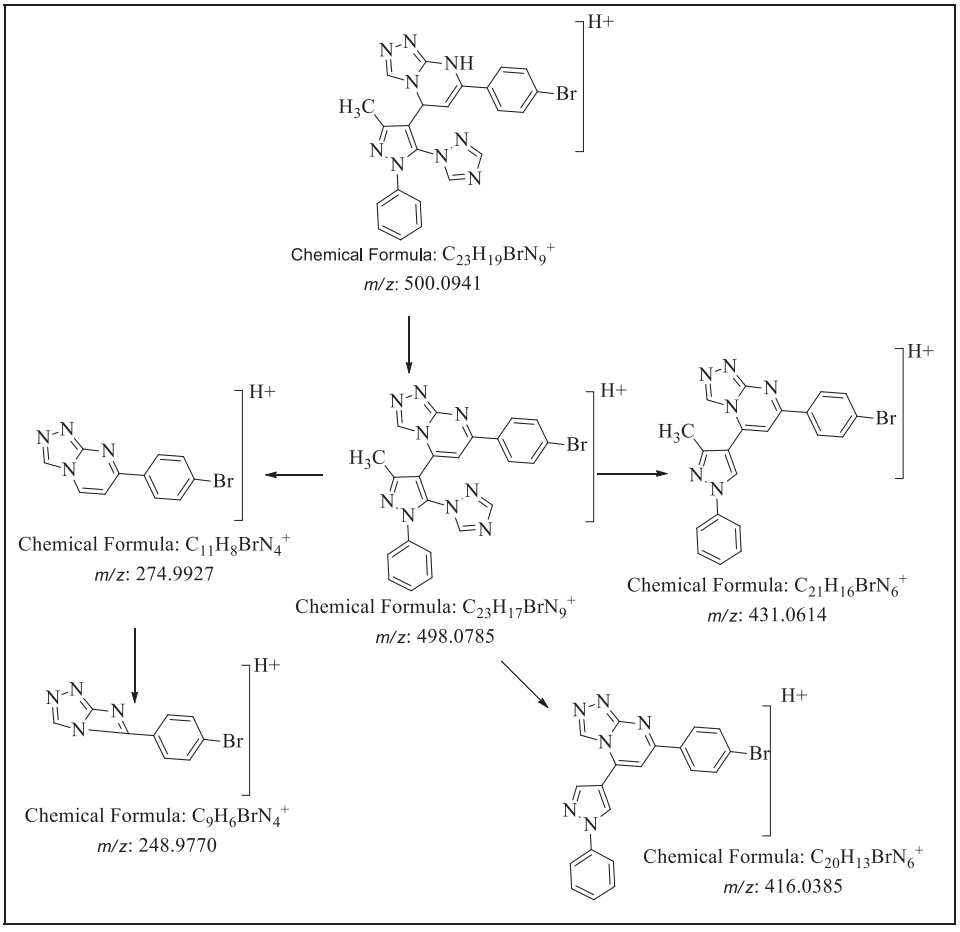

Scheme 2. Fragmentation pathway of the compound **4j**.

Table 3
Salient crystallographic data and structure refinement parameters of the compound **4j.**

Empirical formula	$C_{23}H_{18}BrN_9$
Formula weight	500.37
Crystal system	Triclinic
Space group	*P*-1
T (K)	300
a (Å)	7.8699(4)
b (Å)	11.1217(6)
c (Å)	13.2306(7)
α (°)	99.408(2)
β (°)	103.273(2)
γ (°)	94.005(2)
Z	2
V (Å^3)	1104.96 (10)
D_{calc} (g/cm^3)	1.504
F (0 0 0)	508.0
μ (mm^{-1})	1.892
θ(°)	0.996–26.420
Index ranges	$-9 \le h \le 9$
	$-13 \le k \le 13$
	$-16 \le l \le 16$
N-total	54,660
N-independent	4527
N-observed	3776
Parameters	302
R_1 [*I* > 2 *σ* (*I*)]	0.0483
wR_2 (all data)	0.1375 (4527)
GOF	1.025
CCDC	1,936,467

Table 4
In vitro anti-diabetic activity of compounds **4a-n** on α-glucosidase enzyme.

Entry	Compound	R	IC_{50} (μM)
1	**4a**	H	37.58 ± 0.98
2	**4b**	4-CH_3	48.60 ± 0.37
3	**4c**	4-OCH_3	52.58 ± 0.65
4	**4d**	4-OC_2H_5	27.56 ± 1.20
5	**4e**	4-C_6H_5	43.25 ± 0.54
6	**4f**	4-F	**14.47 ± 0.76**
7	**4g**	3-Cl	**20.30 ± 0.19**
8	**4h**	4-Cl	**12.45 ± 0.59**
9	**4i**	3-Br	30.70 ± 0.25
10	**4j**	4-Br	**25.67 ± 0.43**
11	**4k**	4-I	34.47 ± 0.83
12	**4l**	3-NO_2	**17.27 ± 0.39**
13	**4m**	4-NO_2	35.33 ± 0.51
14	**4n**	4-CN	**23.70 ± 1.50**
15	**Acarbose**	—	**12.68 ± 0.32**

(0.1 U/mL) in phosphate buffer saline was incubated with various concentrations of pyrazole-triazolopyrimidine derivatives at room temperature for 20 min. Then 1.25 mM p-nitrophenyl- α -D-glucopyranoside was added to the mixture as a substrate. The absorbance was measured spectrophotometrically at 405 nm after incubation at room temperature for 30 min. The sample solution was replaced by DMSO as a control. Acarbose was used as a positive control. IC_{50} values were obtained as mean ± SD in triplicates as shown in Table 4.

$$\%\text{Inhibition} = [A_{control} - -A_{sample}]/[A_{control}] \times 100$$

where $A_{control}$ = Absorbance of control; A_{sample} = Absorbance of test compounds

4.2.2. Molecular docking calculations

All the molecules of pyrazole-triazolopyrimidine hybrids (**4a-n**) were built, then converted into 3D structures using Chimera and the structures were energy minimized by using AM1 method. The docking experiment were carried out on α-glucosidase binding site (PDB ID: 3WY1, Resolution: 2.15 A^o) [https://www.rcsb.org/structure/3WY1],

Table 5
Gold score and interactions of the title compounds with receptors of the protein 3WY1.

Entry	Code	Gold score	Interactions	
			H- Bond (Å)	Short contacts (Å)
1	**4a**	57.2	Arg 200(2.32), Gly 228(2.43), Asp 333(2.66).	Phe 166(2.62), Asp 333(2.31), Glu 271(2.37)
2	**4b**	57.99	Arg 200(2.40), Glu 271(2.99), Gly 228(2.47), Asp 333(2.65).	His 105(2.63), Phe 166(2.58), Asp 333(2.33), Glu 271(2.32), Gly 228(2.61).
3	**4c**	35.58	Glu 228(2.17), Asp 333(2.54).	Asp 62(2.58), Phe 297(2.70), Glu 271(2.31,2.42,2.58), Phe 147(2.57)
4	**4d**	63.67	Arg 200(2.37), Glu 271(3.05), Gly 228(2.41), Asp 333(2.62).	His 105(2.64), Phe 166(2.59), Arg 333(2.32), Glu 271(2.39).
5	**4e**	42.98	Gly 228(2.12), Asp 333(2.44)	Phe 147(2.58), Asp 62(2.57), Glu 271(2.28)
6	**4f**	57.30	Arg 200(2.39), Asp 333(2.58), Glu 228(2.43).	Glu 271(2.39), Phe 166(2.59).
7	**4g**	60.98	Gly 228(2.52), Arg 200(2.45), Asp 333(2.57).	His 105(2.63), Phe 166(2.65), Arg 200(2.45), Glu 271(2.38), Gly 228(2.52&2.70).
8	**4h**	89.75	Asp 62(2.57), Asp 333(2.58),(2.97), Asp 202(2.56),(2.89).	His 105(2.55), Phe 166(2.63), The 203(2.76).
9	**4i**	55.86	Arg 200(2.32), Glu 271(2.98), Asp 333(2.68), Gly 228(2.42).	Phe 166(2.60).
10	**4j**	59.15	Arg 200(2.43), Asp 333(2.52), Gly 228(2.39), Glu 271(2.99).	Phe 166(2.59), His 105(2.39), Glu 271(2.34).
11	**4k**	45.78	Glu 271(2.91), Gly 228(2.98), Arg 400(2.59),	Asp 202(2.27),(2.23), Gly 228(2.34).
12	**4l**	63.18	Asp 333(2.58), Arg 200(2.36), Gly 228(2.44),	Phe 166(2.63), Asp 33(2.27), Glu 271(2.34)
13	**4m**	56.48	Gly 228(2.43), Trp 51(2.32), Asp 333(2.69).	His 105(2.63), Phe 166(2.62), Glu 271(2.37), Arg 200(2.32).
14	**4n**	59.96	Gly 228(2.48), Arg 200(2.98).	His 105(2.63), Phe 166(2.63), Glu 271(2.33).

which is a glycoside hydrolase family 13 (GH13), and hydrolysis α-(1 → 4) linked disaccharides. The crude structure of the enzyme was cleaned by removing water molecules, other ligands are refined by competing the incomplete residues, then add hydrogen's and optimized up to the RMS gradient 0.01. The optimized protein was saved as pdb file, which is further used for molecular docking studies. The docking simulation and calculations were carried out by using GOLD 5.6 and HERMES 1.9 interface software [http://www.ccdc.cam.ac.uk/products/gold_suite/] [36]. The active site selection was done by choosing the cavity having the maximum hydrophobic surface area and all the parameters are default settings for docking like rotation angle 30^0, number of placements 30. So that the molecules would be rotated inside the receptor cavity to generate different ligand poses inside the cavity. At the end of the docking process, the minimum energy of interaction between the ligand and 3WY1 protein was obtained as gold

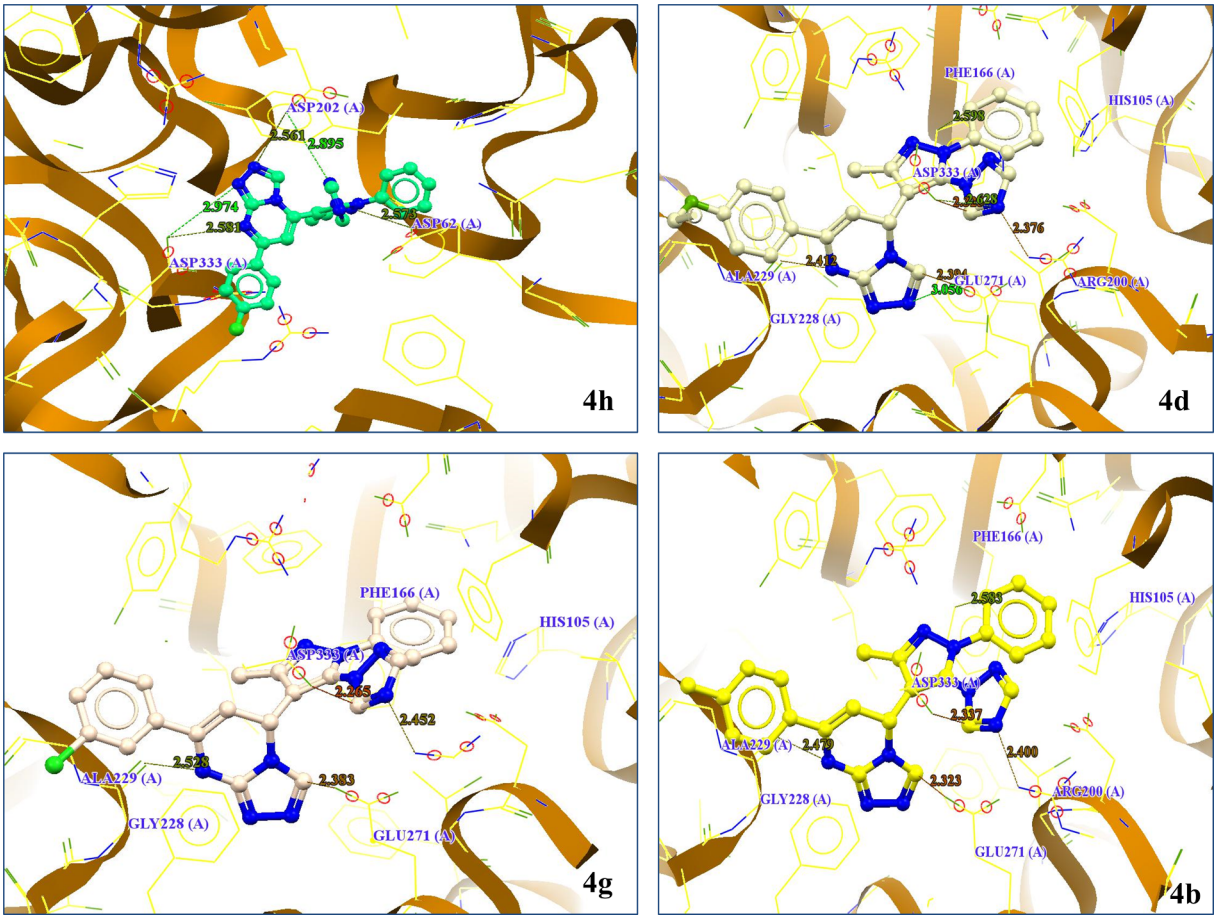

Fig. 4. Representing the binding poses and interactions of ligands **4h**, **4d**, **4g** and **4b** to binding sites of target protein α-glucosidase enzyme (PDB ID: 3WY1).

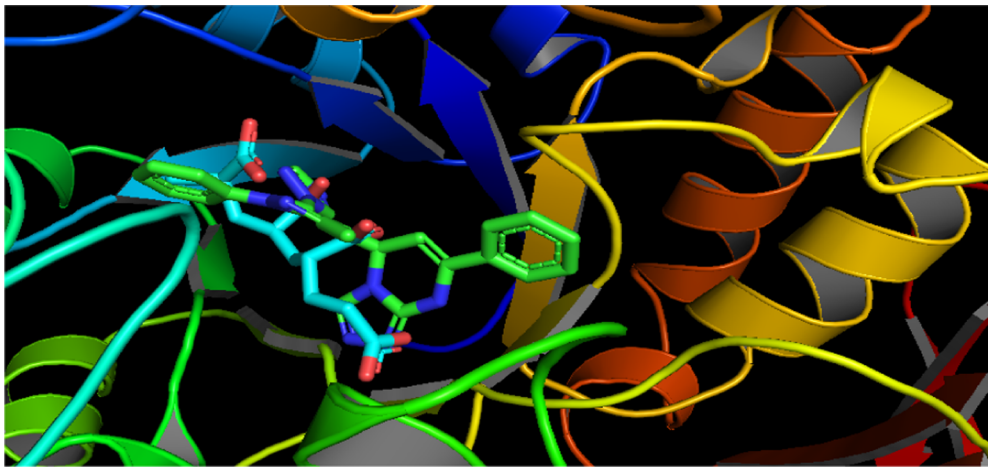

Fig. 5. The compound **4h** and co-crystal ligand at the binding site of the target protein α-glucosidase enzyme (PDB ID: 3WY1).

fitness as a scoring function. The results of the docking scores for each ligand are shown in Table 5. Interactions of 3D and 2D poses between protein and ligands were obtained by Pymol and Ligplot.

4.2.3. ADME predictions

The *in silico* ADME properties of these synthesized compounds were calculated by using the online server preADMET (http://preadmet.bmdrc.org/) [37,38]. The ADMET properties, human intestinal absorption (HIA), Caco-2 cell permeability, Maden Darby Canine Kidney (MDCK) cell permeability, plasma protein binding and blood brain barrier penetration (BBB) were predicted using this program.

Declaration of Competing Interest

The authors declared that there is no conflict of interest.

Acknowledgement

S. B. thanks the Council of Scientific and Industrial Research (CSIR) (02(0300)/17/EMR-II) for financial support. The authors S. B. and V. P.

Table 6
Predicted ADME, Lipinski Parameters.

Entry	MW	*n*-ON	*n*-OHNH	logP(o/w)	*n*-rotb	MV	TPSA	%Abs	n violation
Rule	< **500**	< **10**	< **5**	< **5**	≤**10**	,**500**	< **160**	**100%**	≤**1**
4a	421.47	9	1	2.14	4	367.36	91.29	77.50	0
4b	435.50	9	1	2.59	4	383.92	91.29	77.50	0
4c	451.49	10	1	2.20	5	392.91	100.52	74.32	0
4d	465.52	10	1	2.57	6	409.71	100.52	74.32	0
4e	497.57	9	1	3.94	5	438.77	91.29	77.50	0
4f	439.46	9	1	2.30	4	372.30	91.29	77.50	0
4g	455.91	9	1	2.79	4	380.90	91.29	77.50	0
4h	455.91	9	1	2.82	4	380.90	91.29	77.50	0
4i	500.36	9	1	2.92	4	385.25	91.29	77.50	1
4j	500.36	9	1	2.95	4	385.25	91.29	77.50	1
4k	547.36	9	1	3.22	4	391.35	91.29	77.50	1
4l	466.46	12	1	2.08	5	390.70	137.11	61.70	1
4m	466.46	12	1	2.10	5	390.70	137.11	61.70	1
4n	446.48	10	1	1.90	4	384.22	115.08	69.30	0

M.W: Molecular weight; *n*-ON: Number of hydrogen-bond acceptors (O and N atoms); n OHNH: Number of hydrogen-bond donors (OH and NH groups); logP (o/w): Octanol-water partition coefficient; *n*-rotb: No of Rotatable Bonds; MV: Molecular Volume; TPSA: Topological polar surface area; % ABS: Percentage of absorption (% Abs = 109 − [0.345 × TPSA]).

Table 7
ADME properties predicted for title compounds **4a-n**.

Compounds	[1]Humanintestinalabsorption(%)	[2]*In vitro*Caco-2 cellpermeability (nm/sec)	[3]In vitroMDCK cellpermeability (nm/sec)	[4]*In vitro*plasmaproteinbinding (%)	[5]*In vivo* blood-brainbarrier penetration (C.brain/C.blood)	[6]Skin permeability
4a	96.64	28.60	56.93	100	0.498	−3.63
4b	96.63	29.84	12.85	99.55	0.668	−3.61
4c	96.95	34.08	1.91	94.93	0.389	−3.97
4d	96.88	45.23	0.82	94.45	0.412	−3.85
4e	97.13	36.63	2.22	100.00	0.520	−2.77
4f	96.63	28.785	6.22	90.50	0.619	−3.94
4g	96.77	24.50	5.85	92.72	0.734	−3.68
4h	96.77	24.79	5.32	88.47	0.891	−3.68
4i	97.00	24.36	0.066	89.63	0.787	−3.52
4j	97.00	24.47	0.063	89.85	0.948	−3.53
4k	98.13	24.50	0.413	93.20	0.835	−3.60
4l	97.23	19.57	0.83	94.90	0.102	−3.67
4m	97.23	15.20	0.49	90.23	0.075	−3.67
4n	97.93	17.84	2.24	100.00	0.164	−3.52

Permissible limits: 70–100% Good absorption[1]; > 90 High Permeability[2,3]; > 90% strongly Plasma Protein Binding[4]; > 0.40 CNS active compound[5].

thank the Director, National Institute of Technology, Warangal for providing research facilities. V. P. thanks the MHRD, India for providing research fellowship. The CSIR-IICT Hyderabad Communication No. IICT/Pubs/2019/332.

References

[1] K. Wang, L. Bao, K. Ma, J. Zhang, B. Chen, J. Han, J. Ren, H. Luo, H. Liu, Euro. J. Med. Chem. 127 (2017) 1035–1046, https://doi.org/10.1016/j.ejmech.2016.11.015.
[2] M.G. Salem, Y.M.A. Aziz, M. Elewa, H.A. Elshihawy, M.M. Said, Bioorg. Chem. 79 (2018) 131–144, https://doi.org/10.1016/j.bioorg.2018.04.028.
[3] R. Bhutani, D.P. Pathak, G. Kapoor, A. Husain, R. Kant, Md.A. Iqbal, Bioorg. Chem. 77 (2018) 6–15, https://doi.org/10.1016/j.bioorg.2017.12.037.
[4] C.M.M. Santos, M. Freitas, E. Fernandes, Euro. J. Med. Chem. 157 (2018) 1460–1479, https://doi.org/10.1016/j.ejmech.2018.07.073.
[5] N. Kerru, A.S. Pillay, P. Awolade, P. Singh, Euro. J. Med. Chem. 152 (2018) 436–488, https://doi.org/10.1016/j.ejmech.2018.04.061.
[6] L. Suresh, P. Onkara, P.S. Vijay Kumar, Y. Pydisetty, G.V.P. Chandramouli, Bioorg. Med. Chem. Lett. 26 (2016) 4007–4014, https://doi.org/10.1016/j.bmcl.2016.06.086.
[7] S. Chiba, Biosci. Biotech. Biochem. 61 (1997) 1233–1239, https://doi.org/10.1271/bbb.61.1233.
[8] H.E. Lebovitz, Alpha-glucosidase inhibitors, Endocrinol. Metab. Clin. North Am. 26 (3) (1997) 539–551.
[9] M. Gollapalli, M. Taha, M. Tariq Javid, N. Barak Almandil, F. Rahim, A. Wadood, A. Mosaddik, M. Ibrahim, M.A. Alqahtani, Y.A. Bamarouf, Bioorg. Chem. 85 (2019) 33–48, https://doi.org/10.1016/j.bioorg.2018.12.021.
[10] M. Özil, M. Emirik, S.Y. Etlik, S. Ülker, B. Kahveci, Bioorg. Chem. 68 (2016) 226–235, https://doi.org/10.1016/j.bioorg.2016.08.011.
[11] H. Nikookar, M.M. Khanaposhtani, S. Imanparast, M.A. Faramarzi, P.R. Ranjbar, M. Mahdavi, B. Larijani, Bioorg. Chem. 77 (2018) 280–286, https://doi.org/10.1016/j.bioorg.2018.01.025.
[12] S. Yousuf, K.M. Khan, U. Salar, S. Chigurupati, M. Taj Muhammad, A. Wadood, M. Aldubayan, V. Vijayan, M. Riaz, S. Perveen, J. Euro, Med. Chem. 159 (2018) 47–58, https://doi.org/10.1016/j.ejmech.2018.09.052.
[13] V. Kumar, K. Kaur, G. Kumar Gupta, A. Kumar Sharma, J. Euro, Med. Chem. 69 (2013) 735–753, https://doi.org/10.1016/j.ejmech.2013.08.053.
[14] F. Chaudhry, S. Naureen, M. Ashraf, M. Rashida, B. Jahan, M. Ali Munawar, M. Ain Khan, Bioorg. Chem. (2018), https://doi.org/10.1016/j.bioorg.2018.10.047.
[15] K.L. Kees, J.J. Fitzgerald, K.E. Steiner, J.F. Mattes, B. Mihan, T. Tosi, D. Mondoro, M.L. McCalebr, J. Med. Chem. 39 (1996) 3920–3928, https://doi.org/10.1021/jm960444z.
[16] S. Shu, X. Cai, J. Li, Y. Feng, A. Dai, J. Wang, D. Yang, M.W. Wang, H. Liu, Bioorg. Med. Chem. 24 (2016) 2852–2863, https://doi.org/10.1016/j.bmc.2016.04.053.
[17] S. Shu, A. Dai, J. Wanga, B. Wang, Y. Feng, J. Li, X. Cai, D. Yang, D. Mad, M.W. Wang, H. Liu, Bioorg. Med. Chem. 26 (2018) 1896–1908, https://doi.org/10.1016/j.bmc.2018.02.036.
[18] J.M. Gajbhiye, N.A. More, M.D. Patil, R. Ummanni, S.S. Kotapalli, P. Yogeeswari, D. Sriram, V.H. Masand, Med. Chem. Res. 24 (2015) 2960–2971, https://doi.org/10.1007/s00044-015-1346-4.
[19] C.H. Fang, X.C. Zhou, Rao, Eur. J. Med. Chem. 45 (2010) 4388–4398.
[20] D.A. Pyatakov, A.V. Astakhov, A.N. Sokolov, A.N. Fakhrutdinov, A.N. Fitch, V.B. Rybakov, V.V. Chernyshev, V.M. Chernyshev, Tetrahedron Lett. 58 (2017) 748–754, https://doi.org/10.1016/j.tetlet.2017.01.030.
[21] M. Singh S. Fatma P. Ankit S. Babu Singh J. Singh Tetrahedron Lett. 55 (2014) 525–527. 10.1016/j.tetlet.2013.11.090.
[22] M. Saeedia, M.M. Khanaposhtani, P. Pourrabia, N. Razzaghi, Bioorg. Chem. 83 (2019) 161–169, https://doi.org/10.1016/j.bioorg.2018.10.023.
[23] S. Kumar Avula, A. Khan, N.U. Rehman, M.U. Anwar, Z. Al-Abri, A. Wadood, M. Riaz, R. Csuk, A. Al-Harrasi, Bioorg. Chem. 81 (2018) 98–106, https://doi.org/10.1016/j.bioorg.2018.08.008.

[24] S. Iqbal, M.A. Khan, K. Javaid, R. Sadiq, S. Fazal-ur-Rehman, M.I. Choudhary, F.Z. Basha, Bioorg. Chem. 74 (2017) 72–81, https://doi.org/10.1016/j.bioorg.2017.07.006.
[25] Y. El Bakri, C.H. Lai, J. Sebhaoui, A. Ben Ali, E.M. Essassi, J.T. Mague, J. Mol. Struct. 1184 (2019) 12–24, https://doi.org/10.1016/j.molstruc.2019.01.071.
[26] M.P. DeNinno, S.W. Wright, J.B. Etienne, T.V. Olson, et al., Bioorg. Med. Chem. Lett. 22 (2012) 5721–5726, https://doi.org/10.1016/j.bmcl.2012.06.079.
[27] V.L. Rusinov, I.M. Sapozhnikova, A.M. Bliznik, O.N. Chupakhin, V.N. Charushin, A.A. Spasov, P.M. Vassiliev, V.A. Kuznetsova, A.I. Rashchenko, D.A. Babkov, Arch. Pharm. Chem. Life Sci. 350 (2017) 1600361, https://doi.org/10.1002/ardp.201600361 b) https://russianpatents.com/patent/264/2642432.html.
[28] V.M. Chernyshev, D.A. Pyatakov, A.N. Sokolov, A.V. Astakhov, E.S. Gladkov, S.V. Shishkinab, O.V. Shishkinb, Tetrahedron 70 (2014) 684–701, https://doi.org/10.1016/j.tet.2013.11.090.
[29] Y.A. Mostafa, M.A. Hussein, A.A. Radwan, A.E.H.N. Kfafy, Arch. Pharm. Res. 31 (2008) 279–293, https://doi.org/10.1007/s12272-001-1153-1.
[30] A. Salgado, C. Varela, A.M.G. Collazo, F. García, P. Pevarello, I. Alkorta, J. Elguero, J. Mol. Struct. 987 (2011) 13–24.
[31] I. Łakomska, M. Fandzloch, Coord. Chem. Rev. 327 (2016) 221–241.
[32] V. Pogakua, V.S. Krishna, D. Sriram, K. Rangan, S. Basavojua, Bioorg. Med. Chem. Lett. (2019), https://doi.org/10.1016/j.bmcl.2019.04.026.
[33] V. Pogaku, R.K. Eslavath, G. Dayakar, S.S. Singh, S. Basavoju, Res. Chem. Intermed. 43 (2017) 6079–6098, https://doi.org/10.1007/s11164-017-2978-4.
[34] Z. Gong, Y. Peng, J. Qiu, A. Cao, G. Wang, Z. Peng, Molecules 22 (2017) 1555, https://doi.org/10.3390/molecules22091555.
[35] G. Kiran, D. Krishna Prasad, V. Bakshi, T. Gouthami, Biointerface Res. Appl. Chem. 8 (2018) 3618–3620.
[36] G. Jones, P. Willett, R.C. Glen, A.R. Leach, R. Taylor, J. Mol. Biol. 267 (1997) 727–748, https://doi.org/10.1006/jmbi.1996.0897.
[37] J.C. Cole, J.W.M. Nissink, R. Taylor, Virtual Screening in Drug Discovery, Taylor & Francis CRC Press, Boca Raton, Florida, USA, 2005.
[38] S.K. Lee, I.H. Lee, H.J. Kim, G.S. Chang, J.E. Chung, K.T. No, EuroQSAR 2002 Designing Drugs and Crop Protectants: Processes, Problems and Solutions, Blackwell Publishing, Massachusetts, USA, 2003, pp. 418–420.